

Iterative learning control for a class of multivariable distributed systems with experimental validation

Slawomir Mandra, Krzysztof Galkowski, Andreas Rauh, Harald Aschemann and Eric Rogers

Abstract—This paper develops an iterative learning control design for a class of multiple-input multiple-output systems where a distributed heating system is used as a particular example to experimentally verify the design. The class of systems considered are described by a parabolic partial differential equation, which for control design is approximated by a finite dimensional state-space model obtained by applying the method of integro-differential relations combined with a projection approach. In some cases, including the distributed heating system, this approximation can result in a non-minimum phase system and hence an additional design challenge. In this work, the iterative learning control law is computed in the frequency domain by solving a convex optimization problem and its performance is evaluated in both simulation and experimentation.

Index Terms—Iterative learning control, Feedback control, Distributed system, Multivariable system, Non-minimum phase.

I. INTRODUCTION

Iterative learning control (ILC) has been especially developed for the commonly encountered case where a physical plant or system performs the same finite duration task over and over again. Each execution is termed a trial or pass in the literature, this paper uses the former term and the finite duration of a trial is termed the trial length. Examples include a robot executing a pick and place task, i.e., collect an object (or payload) from a location, transfer it over a finite duration, place it on a moving conveyor (or at a fixed location) under synchronization, return to the starting location for the next payload and so on.

Applications such as pick and place robots can be controlled by specifying a reference trajectory and then applying a control input on each trial whose objective is to enforce close tracking of this trajectory. In turn, this can be formulated by defining the error on each trial as the difference between the reference trajectory (or vector for a multivariable example) and then the design problem is to

use control action to force this error to zero, or to within some acceptable bound, as the number of trials increases.

Research on ILC is well established, where the survey papers [1], [2] are possible sources for an overview of the early research on control law development and applications. Recent applications include marine vibrators [3] and wafer stage semi-conductor manufacturing processes [4]. Also there has been research with experimental verification on design in the presence of uncertainty in model description and the presence of certain forms of disturbances, see, e.g., [5].

Much of the current ILC research is focused on systems that are governed by a set of ordinary differential or discrete equations. Comparatively less effort has addressed ILC design for systems described by partial differential (PDE) equations, also termed distributed parameter systems. One approach to ILC design for such systems is to use semi-group theory, where for linear dynamics frequency domain analysis is also possible, see, e.g., [6]. A typical distributed parameter system to which ILC is applicable would be one where a particular profile is to be established and maintained, e.g., the temperature along a rod, is to be established by repeated finite duration sweeps where the energy applied on the next sweep is dependent on the profile established on the previous sweep.

For many industrial applications, the development of control schemes for distributed parameter systems that can operate in real-time are of particular interest. In this case, there are two fundamentally different approaches, the first of which is to complete the design in the infinite dimensional systems setting and then construct finite-dimensional approximations of low computational complexity for implementation. The alternative is to approximate the distributed parameter dynamics by a finite-dimensional system and then proceed to control design and implementation.

In the latter case, the options include finite volume, finite element or finite difference methods to approximate the distributed parameter dynamics by a system of ordinary differential equations and hence a differential systems state-space model, for further background, see, e.g. [7]. Moreover, if the system is discretized in both space and time then a system of algebraic equations and hence a discrete systems state-space model can be formed. This paper uses another method in the form of integro-differential equations (MIDR) combined with a projection approach [8]. All of these approaches will have an approximation error associated with them and none will be superior in all cases and which to use will depend

Slawomir Mandra is with the Department of Automatics and Measurement Systems, Faculty of Physics, Astronomy and Informatics, Nicolaus Copernicus University, Grudziadzka 5, 87-100 Torun, Poland (e-mail: manslaw@fizyka.umk.pl).

Krzysztof Galkowski is with the Institute of Control and Computation Engineering, University of Zielona Gora, Szafrana 2, 65-516 Zielona Gora, Poland (e-mail: k.galkowski@issi.uz.zgora.pl).

Andreas Rauh and Harald Aschemann are with the Chair of Mechatronics, University of Rostock, Justus-von-Liebig-Weg 6, D-18059 Rostock, Germany (e-mail: andreas.rauh@uni-rostock.de; harald.aschemann@uni-rostock.de).

Eric Rogers is with the School of Electronics and Computer Science, University of Southampton, Southampton SO17 1BJ, UK (e-mail: etar@ecs.soton.ac.uk).

on the particular application under consideration.

Once the finite dimensional model is formed using the MIDR, a new ILC design in the frequency domain for multiple-input multiple-output (MIMO) systems is developed. The design is applicable to models that are either minimum or non-minimum phase, where, as in other areas, non-minimum phase models pose extra design challenges. In [9], three ILC design algorithms for a non-minimum phase MIMO system are developed. The first and second of these are based on the stable inverse of the system model supported by the zero phase-error tracking algorithm [10]. These designs also differ in how the interactions in the MIMO plant are analyzed. The third ILC design is based on \mathcal{H}_∞ -synthesis, first proposed for ILC in [11], with finite preview. In this approach the learning filter of the ILC law is computed for a given Q -filter by solving two coupled Riccati equations. As a result, the calculated filter has the same number of states as the generalized plant. For an uncertain plant model the learning function is found by solving the μ -synthesis problem.

For a non-causal learning filter and/or Q -filter the use of the \mathcal{H}_∞ norm for analysis and design is replaced by the \mathcal{L}_∞ norm in [9]. A new ILC design for MIMO systems is developed based on the \mathcal{L}_∞ norm and convex optimization, where to achieve high control quality, the monotonic convergence condition of the tracking error from trial-to-trial under a given norm is minimized in a frequency range specified by designer e.g. for which the frequency spectrum of a reference signal has many components. The optimization is carried out taking into account restrictions imposed on robustness against unmodeled dynamics of a distributed system as well as a maximum gain (a maximum singular value) of the learning filter to reduce impact of measurement noise and initial condition error. Defining these restrictions requires only providing the values of two scalar parameters. Usually, to obtain the desired ILC performance, it is required to specify weighting functions in the frequency domain [12], [13]. This paper gives substantial new results beyond the conference version [14], including a comprehensive experimental validation. The authors also applied the multivariable norm-optimal iterative learning control to accurate temperature tracking in the heated rod [15].

The nonnegative integer k as a subscript on a vector or scalar valued function, which evolves over the finite trial length, denotes the trial number. Bold letters denote matrices or vectors, bold small letters time-varying column vector signals. The identity matrix with compatible dimension is denoted by \mathbf{I} . Also $\|\cdot\|_\infty$ is the \mathcal{L}_∞ system norm of its discrete-time transfer-function matrix argument and $\bar{\sigma}(\cdot)$ denotes the maximum singular value of a matrix. A symmetric positive (semi-) definite matrix is denoted by $\succ 0$ ($\succeq 0$). Moreover, j is the unit imaginary number and T_s denotes the sampling period.

II. BACKGROUND AND CONTROL DESIGN OBJECTIVES

The most common applications of ILC are still systems described by ordinary differential and/or difference equa-

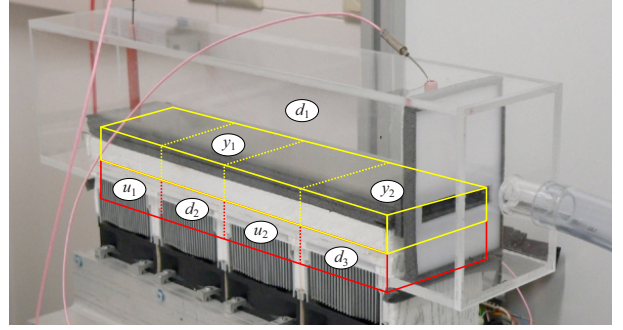


Fig. 1: Experimental setup: an iron rod with rectangular cross-section heated or cooled from bottom by heating elements.

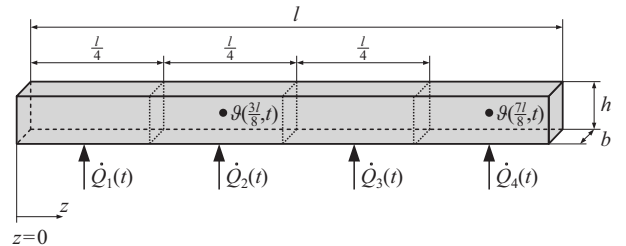


Fig. 2: Schematic representation of the system of Fig. 1 showing the actuator and sensor locations.

tions over a finite duration and operating in a repetitive mode, i.e., a sequence of trials over the finite trial length with resetting to the starting position once each trial is complete, or a stoppage time between the end of one trial and the beginning of the next one. For such systems, the aim is to achieve a specified reference trajectory by using information measured during the previous trial (or a finite number thereof) to update the control action applied on the next trial. The goal is to sequentially improve performance from trial-to-trial and the design problem can be formulated as a tracking problem using a supplied reference representing desired behavior.

Given the progress with design for temporal dynamics, see, e.g., the references cited in the previous section, there is a need to develop ILC for spatio-temporal systems, i.e., dynamics described by PDEs. This paper approaches this problem from the standpoint of first developing a finite-dimensional approximate model of the dynamics as a basis for control law design. The problem considered is establishing a particular temperature profile in a metal rod by repeated sweeps, i.e., trials, of a heating source given a reference profile and sensing and actuating at a finite number of discrete locations along the rod. The resulting design procedure is, however, applicable to all systems modeled by the defining PDE and this issue is considered again in the concluding section of the paper.

The system considered in this paper is shown in Fig. 1 and Fig. 2 gives a schematic diagram with the main variables marked. This system consists of a homogeneous metal rod of length l and a rectangular cross-section (width b , height h , where $b, h \ll l$) that can be heated

or cooled from bottom by four actuators generating heat flows $\dot{Q}_i(t), i = 1, \dots, 4$. All of the side surfaces of the rod are thermally insulated and the top surface is in direct contact with the atmosphere at a temperature of $\vartheta_a(t)$. The edges of the Peltier elements define the sections of the rod and the temperatures at the geometric midpoints (as one case) of the second and fourth sections, i.e., $\vartheta(\frac{3l}{8}, t)$, $\vartheta(\frac{7l}{8}, t)$, are measured and are the controlled system outputs.

In this case, a spatio-temporal temperature distribution $\vartheta(z, t)$ along z -axis, in time t , of the rod can be used to model the dynamics, see [8], which is governed by the PDE

$$\frac{\partial q(z, t)}{\partial z} + \kappa_1 \frac{\partial \vartheta(z, t)}{\partial t} + \kappa_2 \vartheta(z, t) = \mu(z, t) + \kappa_2 \vartheta_a(t), \quad (1)$$

where $q(z, t)$ is the heat flux density given by Fourier's heat conduction law as

$$q(z, t) = -\lambda \frac{\partial \vartheta(z, t)}{\partial z}, \quad (2)$$

with coefficients $\kappa_1 = \rho c_p$ and $\kappa_2 = \frac{\alpha}{h}$ that depend on the density ρ , the specific heat capacity c_p , the convective heat transfer coefficient α , the height h of the rod and λ , which is the heat conductivity. The input function $\mu(z, t)$ models the spatial distribution of the heat flux transferred by the actuators

$$\mu(z, t) = \sum_{i=1}^4 a_i(z) \dot{Q}_i(t), \quad (3)$$

where i enumerates the rod sections, and

$$a_i(z) = \begin{cases} \frac{4}{bh} & \text{for } z \in [z_{i-1}, z_i], \\ 0 & \text{otherwise.} \end{cases} \quad (4)$$

The positions $z_i = i\frac{l}{4}$, $i = 1, 2, 3, 4$, are the edges of the actuators. Since the side surfaces of the rod are isolated, the boundary conditions for the heat flux density $q(z, t)$ are: $q(0, t) = \bar{q}_0(t) = 0$ and $q(l, t) = \bar{q}_l(t) = 0$. In general, the initial ($t = 0$) temperature distribution in the rod can be specified as $\vartheta(z, 0) = \bar{\vartheta}_0(z)$ or, in particular, as the initial ambient temperature i.e. $\vartheta(z, 0) = \vartheta_a(0)$. All simulation and experimental results given in this paper use this last condition.

Note 1. *As given above, the experimental setup satisfies $b, h \ll l$. Consequently the temperature mainly changes along the longitudinal direction of the rod (l) and the changes in the orthogonal directions (b, h) are negligible. This justifies the 1-D modeling assumption, for further details, see, e.g., [16].*

Substituting (2) into (1) gives the parabolic PDE that governs the spatially distributed temperature in the rod. Next, the method of integro-differential relations (MIDR) combined with the projection approach [8] is used to construct the finite dimensional approximate model used for design and experimental verification in the rest of this paper. Moreover, this method can be applied to any system described by the PDE considered. The relative merits

of this model approximation method against alternatives is considered again at the end of this section and in the concluding section of this paper.

In the application of MIDR to the heating process, the temperature profile in each section of the rod is approximated by a polynomials of degree M and hence

$$\tilde{\vartheta}(z, t) = \sum_{i=1}^4 \sum_{m=0}^M b_{i,m,M}(z) \theta_{i,m,M}(t), \quad (5)$$

where the functions $b_{i,m,M}(z)$ are the Bernstein polynomials

$$b_{i,m,M}(z) = \begin{cases} b_i^{m,M}(z) & \text{for } z \in [z_{i-1}, z_i], \\ 0 & \text{otherwise,} \end{cases} \quad (6)$$

$$b_i^{m,M}(z) = \binom{M}{m} \left(\frac{z - z_{i-1}}{z_i - z_{i-1}} \right)^m \left(\frac{z_i - z}{z_i - z_{i-1}} \right)^{M-m}$$

and $\theta_{i,m,M}(t)$ are the unknown time-dependent coefficients. The temperature distribution continuity between neighbouring segments i and $i + 1$ is guaranteed by the assumption that

$$\theta_{i,0,M}(t) = \theta_{i-1,M,M}(t), \quad i = 2, 3, 4. \quad (7)$$

The finite-dimensional state-space model approximation of the dynamics is obtained by following the procedure given in [8]. In application, this method requires the selection of the degree M of the Bernstein polynomials and this is application specific. In the considered case, the ambient temperature above the rod is homogeneous and the initial temperature distribution of the rod is equal to the ambient temperature. The heat flows transferred by the actuators are also homogeneous. Also it is assumed that the reference temperature is smooth and hence the temperature distribution in each segment of the rod is also smooth. Based on these facts, $M = 3$ is used and a state-space model of the following form is obtained

$$\dot{\mathbf{x}}(t) = \mathbf{A}_c \mathbf{x}(t) + \mathbf{B}_c \mathbf{u}_c(t) + \mathbf{E}_c \vartheta_a(t), \quad (8)$$

where

$$\mathbf{x}(t) = [\mathbf{x}_1(t) \quad \mathbf{x}_2(t) \quad \mathbf{x}_3(t) \quad \mathbf{x}_4(t)]^T$$

and

$$\mathbf{x}_1(t) = \begin{bmatrix} \theta_{1,0,3}(t) \\ \theta_{1,1,3}(t) \\ \theta_{1,2,3}(t) \\ \theta_{1,3,3}(t) \end{bmatrix}^T, \quad \mathbf{x}_2(t) = \begin{bmatrix} \theta_{2,1,3}(t) \\ \theta_{2,2,3}(t) \\ \theta_{2,3,3}(t) \end{bmatrix}^T,$$

$$\mathbf{x}_3(t) = \begin{bmatrix} \theta_{3,1,3}(t) \\ \theta_{3,2,3}(t) \\ \theta_{3,3,3}(t) \end{bmatrix}^T, \quad \mathbf{x}_4(t) = \begin{bmatrix} \theta_{4,1,3}(t) \\ \theta_{4,2,3}(t) \\ \theta_{4,3,3}(t) \end{bmatrix}^T,$$

$$\mathbf{u}_c(t) = [\dot{Q}_1(t) \quad \dot{Q}_2(t) \quad \dot{Q}_3(t) \quad \dot{Q}_4(t)]^T.$$

The output equation to complete the state-space model is obtained by evaluating (5) for the temperature sensor positions $z = \frac{3l}{8}, \frac{7l}{8}$ and hence

$$\mathbf{y}(t) = \mathbf{C}_c \mathbf{x}(t), \quad (9)$$

Combining these last two state-space models gives

$$\begin{aligned} \mathbf{z}_{k+1}(p+1) &= \mathbf{A}_a \mathbf{z}_{k+1}(p) + \mathbf{B}_a \mathbf{u}_{k+1}(p), \\ \mathbf{y}_{k+1}(p) &= \mathbf{C}_a \mathbf{z}_{k+1}(p), \end{aligned} \quad (15)$$

where

$$\begin{aligned} \mathbf{A}_a &= \begin{bmatrix} \mathbf{A} & \mathbf{B}\mathbf{C}_d \\ \mathbf{0} & \mathbf{A}_d \end{bmatrix}, \quad \mathbf{z}_{k+1}(p) = \begin{bmatrix} \mathbf{x}_{k+1}(p) \\ \boldsymbol{\varepsilon}_{k+1}(p) \end{bmatrix}, \\ \mathbf{B}_a &= \begin{bmatrix} \mathbf{B} \\ \mathbf{0} \end{bmatrix}, \quad \mathbf{C}_a = [\mathbf{C} \quad \mathbf{0}]. \end{aligned}$$

Estimation of the state and equivalent disturbance vectors is by the Luenberger observer

$$\begin{aligned} \hat{\mathbf{z}}_{k+1}(p+1) &= \mathbf{A}_a \hat{\mathbf{z}}_{k+1}(p) + \mathbf{B}_a \mathbf{u}_{k+1}(p) \\ &\quad + \mathbf{K}_L (\mathbf{y}_{k+1}(p) - \mathbf{C}_a \hat{\mathbf{z}}_{k+1}(p)), \end{aligned} \quad (16)$$

where $\hat{\mathbf{z}}_{k+1}(p) = [\hat{\mathbf{x}}_{k+1}^T(p) \quad \hat{\boldsymbol{\varepsilon}}_{k+1}^T(p)]^T$ is the observer state vector and $\mathbf{K}_L = [\mathbf{K}_{L1}^T \quad \mathbf{K}_{L2}^T]^T$ is the observer gain matrix. Also the estimated equivalent disturbance vector is calculated as

$$\hat{\boldsymbol{\delta}}_{k+1}(p) = \mathbf{C}_d \hat{\boldsymbol{\varepsilon}}_{k+1}(p). \quad (17)$$

The current trial feedback control loop (see Fig.3) constructs the plant input as

$$\mathbf{u}_{k+1}(p) = \mathbf{N} \mathbf{w}_{k+1}(p) - \mathbf{K}_s \hat{\mathbf{x}}_{k+1}(p) - \hat{\boldsymbol{\delta}}_{k+1}(p), \quad (18)$$

where \mathbf{N} is the static feedforward gain matrix and $\mathbf{w}_{k+1}(p)$ represents a signal by which the ILC action and the reference trajectory are applied, as specified below. Routine manipulations give the following state-space model description of the real-time control dynamics

$$\begin{aligned} \boldsymbol{\chi}_{k+1}(p+1) &= \mathbf{A}_{cl} \boldsymbol{\chi}_{k+1}(p) + \mathbf{B}_{cl} \mathbf{w}_{k+1}(p) + \mathbf{E}_{cl} \mathbf{d}_{k+1}(p), \\ \mathbf{y}_{k+1}(p) &= \mathbf{C}_{cl} \boldsymbol{\chi}_{k+1}(p), \end{aligned} \quad (19)$$

where

$$\begin{aligned} \mathbf{A}_{cl} &= \begin{bmatrix} \mathbf{A} & -\mathbf{B}\mathbf{K}_s & -\mathbf{B}\mathbf{C}_d \\ \mathbf{K}_{L1}\mathbf{C} & \mathbf{A} - \mathbf{B}\mathbf{K}_s - \mathbf{K}_{L1}\mathbf{C} & \mathbf{0} \\ \mathbf{K}_{L2}\mathbf{C} & -\mathbf{K}_{L2}\mathbf{C} & \mathbf{A}_d \end{bmatrix}, \\ \mathbf{B}_{cl} &= \begin{bmatrix} \mathbf{B}\mathbf{N} \\ \mathbf{B}\mathbf{N} \\ \mathbf{0} \end{bmatrix}, \quad \mathbf{E}_{cl} = \begin{bmatrix} \mathbf{E} \\ \mathbf{0} \\ \mathbf{0} \end{bmatrix}, \quad \boldsymbol{\chi}_{k+1}(p) = \begin{bmatrix} \mathbf{x}_{k+1}(p) \\ \hat{\mathbf{x}}_{k+1}(p) \\ \hat{\boldsymbol{\varepsilon}}_{k+1}(p) \end{bmatrix}, \\ \mathbf{C}_{cl} &= [\mathbf{C} \quad \mathbf{0} \quad \mathbf{0}]. \end{aligned}$$

Let

$$\mathbf{y}^{\text{ref}}(p) = \begin{bmatrix} y^{\text{ref}1}(p) \\ y^{\text{ref}2}(p) \end{bmatrix} \quad (20)$$

denotes the reference vector. Then the tracking error vector on trial k is

$$\mathbf{e}_k(p) = \mathbf{y}^{\text{ref}}(p) - \mathbf{y}_k(p). \quad (21)$$

The vector generated by the ILC law and the reference trajectory together form

$$\mathbf{w}_{k+1}(p) = \mathbf{y}^{\text{ref}}(p) + \mathbf{v}_{k+1}(p) \quad (22)$$

with

$$\mathbf{v}_{k+1}(p) = \mathbf{Q}(q)(\mathbf{v}_k(p) + \mathbf{L}(q)\mathbf{e}_k(p)), \quad (23)$$

where q is the forward time-shift operator $q\mathbf{e}_k(p) \equiv \mathbf{e}_k(p+1)$. This control law is extensively used in ILC, see, e.g., [1], both in simulation and experimental verification, where $\mathbf{Q}(q)$ is often termed the robustness filter or Q -filter and $\mathbf{L}(q)$ is the learning filter. The detailed structure of $\mathbf{Q}(q)$ and $\mathbf{L}(q)$ is application dependent and the rest of this section develops a design without a detailed structure for either of these filters, where $\mathbf{L}(q)$ must be of FIR structure to give a convex optimization problem. Then in the next section the selection of the Q -filter and the learning filter to advantage for a particular example is given for the heating process, supported by experimental results.

Design of the state feedback matrix \mathbf{K}_s can be completed in many ways given the required controllability assumption. In this paper, the route is by minimizing the linear quadratic cost function

$$J_s = \sum_{p=0}^{\infty} \left(\mathbf{x}_{k+1}^T(p) \mathbf{Q}_s \mathbf{x}_{k+1}(p) + \mathbf{u}_{k+1}^T(p) \mathbf{R}_s \mathbf{u}_{k+1}(p) \right), \quad (24)$$

where $\mathbf{Q}_s \succeq 0$ and $\mathbf{R}_s \succ 0$ are appropriately chosen weighting matrices. This solution involves the discrete-time matrix Riccati equation

$$\mathbf{A}^T \mathbf{P}_s (\mathbf{I} - \mathbf{B}(\mathbf{B}^T \mathbf{P}_s \mathbf{B} + \mathbf{R}_s)^{-1} \mathbf{B}^T \mathbf{P}_s) \mathbf{A} + \mathbf{Q}_s = \mathbf{P}_s, \quad (25)$$

whose solution \mathbf{P}_s gives \mathbf{K}_s as

$$\mathbf{K}_s = (\mathbf{B}^T \mathbf{P}_s \mathbf{B} + \mathbf{R}_s)^{-1} (\mathbf{B}^T \mathbf{P}_s \mathbf{A}). \quad (26)$$

By the separation principle, the observer gain matrix can be designed independent of \mathbf{K}_s . Again the minimizing quadratic cost function route is used, i.e.,

$$J_o = \sum_{p=0}^{\infty} \left(\check{\mathbf{z}}_{k+1}^T(p) \mathbf{Q}_o \check{\mathbf{z}}_{k+1}(p) + \check{\mathbf{y}}_{k+1}^T(p) \mathbf{R}_o \check{\mathbf{y}}_{k+1}(p) \right), \quad (27)$$

where $\check{\mathbf{z}}_{k+1}(p) = \mathbf{z}_{k+1}(p) - \hat{\mathbf{z}}_{k+1}(p)$ is the state estimation error vector, $\check{\mathbf{y}}_{k+1}(p) = \mathbf{y}_{k+1}(p) - \hat{\mathbf{y}}_{k+1}(p)$ is the output estimation error vector and $\mathbf{Q}_o \succeq 0$ and $\mathbf{R}_o \succ 0$ are appropriately chosen weighting matrices. The solution matrix \mathbf{P}_o of the following discrete-time matrix Riccati equation

$$\mathbf{A}\mathbf{P}_o(\mathbf{I} - \mathbf{C}^T(\mathbf{C}\mathbf{P}_o\mathbf{C}^T + \mathbf{R}_o)^{-1}\mathbf{C}\mathbf{P}_o)\mathbf{A}^T + \mathbf{Q}_o = \mathbf{P}_o \quad (28)$$

gives

$$\mathbf{K}_L = ((\mathbf{C}\mathbf{P}_o\mathbf{C}^T + \mathbf{R}_o)^{-1}(\mathbf{C}\mathbf{P}_o\mathbf{A}^T))^T. \quad (29)$$

The static feedforward gain matrix \mathbf{N} in (18) can, if required, be chosen as the inverse of the DC gain matrix of the feedback control loop to reduce the steady-state error in the feedback loop. This control action is particularly significant only on the first trial.

For the ILC design, the frequency domain description of (19) is used, i.e., on applying the z -transform

$$\mathbf{Y}_{k+1}(z) = \mathbf{P}(z)(\mathbf{V}_{k+1}(z) + \mathbf{Y}^{\text{ref}}(z)) + \tilde{\mathbf{P}}(z)\mathbf{D}(z), \quad (30)$$

where

$$\mathbf{P}(z) = \mathbf{C}_{cl}(z\mathbf{I} - \mathbf{A}_{cl})^{-1}\mathbf{B}_{cl}, \quad (31)$$

$$\tilde{\mathbf{P}}(z) = \mathbf{C}_{cl}(z\mathbf{I} - \mathbf{A}_{cl})^{-1}\mathbf{E}_{cl}. \quad (32)$$

In ILC the z -transform, defined over an infinite horizon signal, is an approximation due to the finite trial length and hence a large number of samples per duration time is assumed [19].

The ILC law (23) in the z -domain (where the dependence on z is suppressed when the meaning is clear) is

$$\mathbf{V}_{k+1} = \mathbf{Q}(\mathbf{V}_k + \mathbf{L}\mathbf{E}_k). \quad (33)$$

and

$$\mathbf{E}_k = \mathbf{Y}^{\text{ref}} - \mathbf{Y}_k. \quad (34)$$

Stability of the plant dynamics \mathbf{P} is guaranteed by the feedback control loop and monotonic trial-to-trial error convergence under a given norm is established by the following well known result, see, e.g. [1].

Lemma 1. *Suppose that an ILC law of the form (33) is applied to a MIMO system described by (30). Suppose also that*

$$\|\mathbf{P}\mathbf{Q}(\mathbf{P}^{-1} - \mathbf{L})\|_{\infty} = \gamma < 1, \quad (35)$$

then the ILC dynamics

$$\begin{aligned} \mathbf{E}_{k+1} = & \mathbf{P}\mathbf{Q}(\mathbf{P}^{-1} - \mathbf{L})\mathbf{E}_k \\ & + (\mathbf{I} - \mathbf{P}\mathbf{Q}\mathbf{P}^{-1})((\mathbf{I} - \mathbf{P})\mathbf{Y}^{\text{ref}} - \tilde{\mathbf{P}}\mathbf{D}) \end{aligned} \quad (36)$$

is stable and the trial-to-trial tracking error converges monotonically under a given norm, i.e.,

$$\|\mathbf{E}_{\infty} - \mathbf{E}_{k+1}\|_2 \leq \gamma \|\mathbf{E}_{\infty} - \mathbf{E}_k\|_2, \quad (37)$$

to

$$\begin{aligned} \mathbf{E}_{\infty} = & (\mathbf{I} - \mathbf{P}\mathbf{Q}(\mathbf{P}^{-1} - \mathbf{L}))^{-1}(\mathbf{I} - \mathbf{P}\mathbf{Q}\mathbf{P}^{-1}) \\ & \cdot ((\mathbf{I} - \mathbf{P})\mathbf{Y}^{\text{ref}} - \tilde{\mathbf{P}}\mathbf{D}). \end{aligned} \quad (38)$$

Given (38), it follows immediately that perfect tracking for all \mathbf{Y}^{ref} and \mathbf{D} is possible if $\mathbf{Q} = \mathbf{I}$. In applications a Q -filter in form of a zero-phase low-pass filter with unity magnitude at low frequency is often used to improve learning system robustness to uncertainty in the plant model. This is at the cost of not satisfying the perfect tracking property, see, e.g. [1]. For the application area considered in this paper, the use of an appropriately chosen Q -filter is especially important because the model used for design is an approximation of the PDE dynamics.

In general, the ILC design problem is to select the Q -filter and the learning filter to achieve high tracking accuracy over a wide frequencies range, fast and monotonic trial-to-trial error convergence under a given norm, appropriate robustness of the control system to modelling errors and low sensitivity to measurement noise and initial conditions. These are conflicting requirements (to some degree) and in this paper the following convex optimization problem in the frequency domain, which guarantees monotonic convergence of the tracking error vector from trial-to-trial under a given norm is proposed. This assumes the frequency responses $\mathbf{Q}(e^{j\omega_i T_s})$ of the Q -filter have been constructed for the application under consideration, where a particular example is given in the next section.

The new ILC design algorithm is

$$\underset{\mathbf{L}}{\text{minimize}} \quad \sum_{\omega_i=\omega_{r1}}^{\omega_{r2}} \bar{\sigma}(\mathbf{M}(e^{j\omega_i T_s}))$$

subject to:

$$\begin{aligned} \bar{\sigma}(\mathbf{M}(e^{j\omega_i T_s})) & \leq M_{\max}, \quad \forall \omega_i \in [\omega_1 < \omega_2 < \dots < \omega_N] \\ \bar{\sigma}(\mathbf{L}(e^{j\omega_i T_s})) & \leq L_{\max}, \quad \forall \omega_i \in [\omega_1 < \omega_2 < \dots < \omega_N] \end{aligned} \quad (39)$$

where

$$\mathbf{M}(e^{j\omega_i T_s}) = \mathbf{P}(e^{j\omega_i T_s})\mathbf{Q}(e^{j\omega_i T_s})(\mathbf{P}^{-1}(e^{j\omega_i T_s}) - \mathbf{L}(e^{j\omega_i T_s})). \quad (40)$$

This algorithm is for MIMO systems and is a major contribution of this paper. The optimization parameter $0 < M_{\max} < 1$ is an upper bound on convergence rate γ (see (35)) and has been introduced to increase robustness against unmodeled dynamics. The second constraint of (39) limits the maximum gain (the maximum singular value) of the learning filter to an appropriately selected value L_{\max} , which again depends on the application considered. It has been added to reduce the impact of measurement noise and initial conditions on performance. In [12], [13] this problem has been solved by the introduction of a weighting function defined in frequency domain, which complicates the design and is not required in this approach.

The constraints of (39) should be satisfied for all ω in $[0, \omega_N]$, where ω_N is the Nyquist frequency. This can be relaxed such that only a finite, but large, number of logarithmically spaced angular frequencies ω_i are considered (angular frequency gridding). A consequence of limiting the maximum singular value of the learning filter could be a reduction in the trial-to-trial convergence speed, potentially over a wide range of frequencies.

For a given frequency ω_i , the convergence speed depends on $\bar{\sigma}(\mathbf{M}(e^{j\omega_i T_s}))$. In particular, reducing this value gives faster the trial-to-trial error convergence. Moreover, in applications it could be important to obtain fast monotonic trial-to-trial error convergence rate of the tracking error under a specified norm over the frequency range for which the frequency spectrum of the reference signal has many components. In the optimization problem above, this is achieved by minimizing the sum of all $\bar{\sigma}(\mathbf{M}(e^{j\omega_i T_s}))$ between the lower ω_{r1} and upper ω_{r2} limits of the angular frequency range for which the reference signal spectrum has components with significant magnitude, which is again application dependent.

IV. SIMULATION AND EXPERIMENTAL VERIFICATION

The section gives the results from validation of the algorithm developed in the previous section applied to the MIMO heating system of Section II. The location of the input and output signals of the approximate plant model (10) are marked in Fig. 1 using the following notation: $u_1 \equiv \dot{Q}_1(t)$ and $u_2 \equiv \dot{Q}_3(t)$ are the first and second entry of the input vector signal $\mathbf{u}(t)$, respectively; $d_1 \equiv \vartheta_a(t)$, $d_2 \equiv \dot{Q}_2(t)$ and $d_3 \equiv \dot{Q}_4(t)$ are the entries

in the disturbance vector signal $\mathbf{d}(t)$; $y_1 \equiv \vartheta(\frac{3l}{8}, t)$ and $y_2 \equiv \vartheta(\frac{7l}{8}, t)$ are, respectively, the first and second entry of the output vector $\mathbf{y}(t)$.

The numerical values of the experimental setup plant model parameters are as follows: $l = 0.320$ m, $b = 0.040$ m, $h = 0.012$ m, $\rho = 7800$ kg/m³, $c_p = 420$ J/(kg·K), $\alpha = 150$ W/(m²·K) and $\lambda = 55$ W/(m·K). For these values a minimal realisation of (10) was constructed, resulting in a model with 10 states, which is non-minimum phase with two invariant zeros, both at $s = 0.1011$. Using the exact discretization method with a sampling period of $T_s = 1$ s results in a state-space model of the form (12), again with $\mathbf{x}_{k+1}(p) \in \mathbb{R}^{10}$. This model is also non-minimum phase with two invariant zeros both at $z = 1.1065$. As in other areas of linear systems, non-minimum phase zeros have particular effects on ILC performance, see, e.g., [20].

The ambient temperature is a non-repeatable disturbance that cannot be compensated by the ILC law. This temperature is slow-varying and therefore the disturbance observer can be used to compensate for its effect. For this reason, the disturbance model (14) is chosen as integral action, i.e., $\mathbf{A}_d = \mathbf{C}_d = \mathbf{I}$.

Each controller in the overall ILC design is designed separately based on the plant model (12). Both the state feedback gain matrix \mathbf{K}_s and the state and disturbance Luenberger observer gain matrix \mathbf{K}_L have been calculated using the optimization setting given in Section III. To enforce a compromise between fast dynamics and the suppression of high frequency noise, the weighting matrices in (24) and (27) have been taken as $\mathbf{Q}_s = \mathbf{C}^T \mathbf{C}$, $\mathbf{R}_s = 0.05\mathbf{I}$, $\mathbf{Q}_o = \text{diag}(\mathbf{I}, 2\mathbf{I})$ and $\mathbf{R}_o = \mathbf{I}$. This results in

$$\mathbf{K}_s = \begin{bmatrix} -0.0439 & -0.0491 \\ 0.3642 & 0.1032 \\ 0.2670 & 0.2436 \\ -0.2905 & -0.1920 \\ 0.2442 & 0.1252 \\ 0.3569 & 0.3568 \\ 0.2495 & 0.3114 \\ 0.1471 & 0.2493 \\ -0.0498 & -0.4204 \\ -0.1456 & 0.8236 \end{bmatrix}^T, \quad \mathbf{K}_L = \begin{bmatrix} -0.6349 & 0.3741 \\ 0.7399 & -0.4144 \\ 0.9401 & -0.4358 \\ -0.6769 & 0.3089 \\ -0.1206 & 0.2423 \\ 0.4635 & -0.0255 \\ -0.0629 & 0.5887 \\ 0.1947 & 0.7508 \\ -0.5103 & -0.5924 \\ -0.1081 & 0.7205 \\ 0.9831 & -0.4295 \\ 0.4307 & 0.9887 \end{bmatrix}.$$

The choice of the weighting matrices used is a matter for judgement based on the particular example under consideration, the set here demonstrates that such matrices can be found. Moreover, any pole placement with an observer design method can be used. These matrices are used in the simulation and experimental results given below and it is also noted that in detailed design they may have to be reselected to obtain the required response for a given example.

To achieve a small steady state error vector on the first trial, the static feedforward gain matrix (see Fig. 3) has been taken as the inverse of the DC gain matrix of the closed-loop feedback control system and hence

$$\mathbf{N} = \begin{bmatrix} 4.6935 & -2.4303 \\ 1.5513 & 4.6324 \end{bmatrix}.$$

Again other choices are possible depending on the application considered and the performance requirements.

The design of the ILC law begins with the specification of the Q and L -filters. As one example, the design below is based on the premise that the current trial feedback control loop results in controlled dynamics with a transfer-function matrix \mathbf{P} that is approximately diagonal over the frequency range of interest. In which case, diagonal structures can be selected for the Q and L -filters.

The particular structure of the Q and L -filters considered first have the form

$$\mathbf{Q}(q) = \text{diag}(Q_1(q), Q_2(q)), \quad (41)$$

and

$$\mathbf{L}(q) = \text{diag}(L_1(q), L_2(q)). \quad (42)$$

The entries of the Q -filter are in the form of low-pass, Butterworth filter of order n_{Qm} applied in zero-phase form, resulting in a $2n_{Qm}$ -th order zero-phase low-pass filter written as

$$Q_m(q) = \frac{b_{0m} + b_{1m}q^{-1} + b_{2m}q^{-2} + \dots + b_{n_{Qm}}q^{-n_{Qm}}}{1 + a_{1m}q^{-1} + a_{2m}q^{-2} + \dots + a_{n_{Qm}}q^{-n_{Qm}}} \cdot \frac{b_{0m} + b_{1m}q + b_{2m}q^2 + \dots + b_{n_{Qm}}q^{n_{Qm}}}{1 + a_{1m}q + a_{2m}q^2 + \dots + a_{n_{Qm}}q^{n_{Qm}}}, \quad (43)$$

where $m = 1, 2$. The learning filter matrix entries are formed from non-causal finite impulse response filters of order n_{Lm} , i.e.,

$$L_m(q) = l_{1m}q + l_{2m}q^2 + \dots + l_{n_{Lm}}q^{n_{Lm}}. \quad (44)$$

Consider the matrix \mathbf{P} for the controlled current trial feedback loop for the heating process written in the form

$$\mathbf{P} = \begin{bmatrix} P_{11} & P_{12} \\ P_{21} & P_{22} \end{bmatrix}.$$

Fig. 4 shows the Bode gain plots for each of the four entries in this 2×2 frequency response matrix, where the magnitudes of the off-diagonal entries are smaller than those on the diagonal. Hence (41) is further simplified to $\mathbf{Q} = Q\mathbf{I}$ and the remaining task is to select the filter order n_{Qm} , chosen to be 2 and the cut-off frequency of this filter is chosen as 0.1 rad/s, where above this frequency the feedback control loop significantly damps the input vector $\mathbf{w}_{k+1}(p)$.

The maximum singular value of \mathbf{P} as well as magnitudes of P_{11} and P_{22} at this frequency are $\bar{\sigma}(\mathbf{P}(e^{j0.1T_s})) \approx |P_{11}(e^{j0.1T_s})| \approx |P_{22}(e^{j0.1T_s})| \approx 0.05$. Given that $|P_{11}|$ and $|P_{22}|$ have similar values for frequencies from 10^{-4} rad to the Nyquist frequency, therefore $Q_1 = Q_2$ is assumed. The Bode diagram with $Q = Q_1 = Q_2$ is given in Fig. 5.

The new ILC design has been applied in simulation to the heating process of Section II and the result experimentally validated. The results are given and discussed next. Then the relative performance against alternatives is described.

All optimization problems in the results that follow were solved using the MATLAB based software CVX and

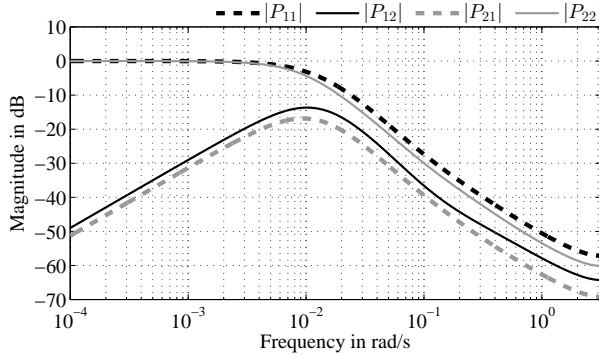


Fig. 4: Magnitudes of the entries in transfer-function matrix describing the dynamics of the feedback control loop.

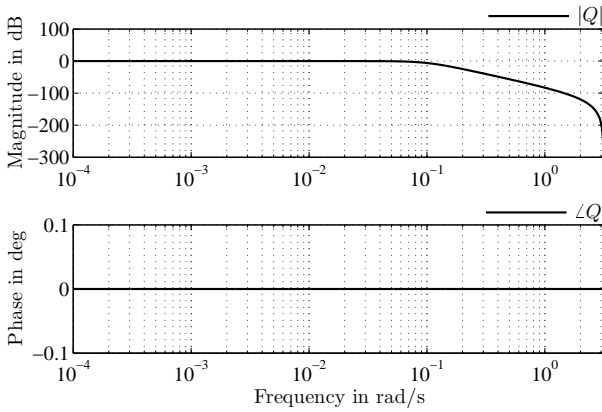


Fig. 5: Bode diagram of the first (and the second) entry of the Q -filter.

SDPT3 for 1000 values of logarithmically spaced frequencies ω_i in the range $[10^{-4}, \omega_N = \frac{\pi}{T_s}]$ rad/s and $M_{\max} = 0.9$ was chosen to obtain acceptable robustness.

Singular values of \mathbf{P} below the frequency 10^{-4} rad/s and between the frequency samples ω_i do not change significantly. This guarantees that the model of the current trial feedback loop is appropriately determined and the constraints of (39) are satisfied below 10^{-4} rad/s and between the frequency samples ω_i .

The orders of $L_1(q)$ and $L_2(q)$ of the learning filter (42), relative to the order of the plant model (12), have been taken as $n_{L1} = n_{L2} = 10$. The model of the feedback control loop (19) or (31) is 22th order, where the 12 additional states are introduced by the state and disturbance observer (16).

One of the advantages relative to alternatives (the most relevant are considered later in this section) of the new design (39) is the ability to achieve fast trial-to-trial error convergence over a frequency range of interest, i.e., ω_{r1} and ω_{r2} , respectively, as defined at the end of the previous section. In the current design these are selected by examining the frequency spectrum of the reference signals. Fig. 7 (top plot) shows the reference trajectories (black and gray solid line) applied during all design studies

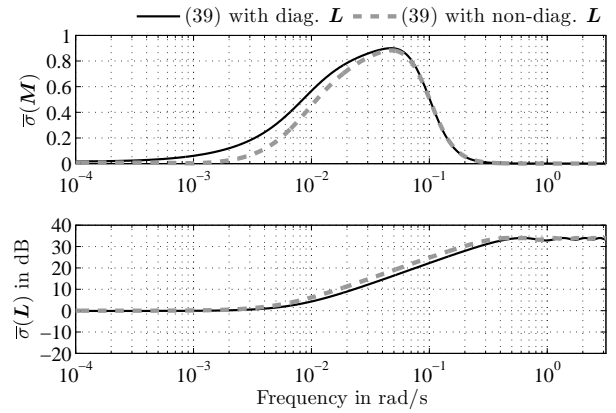


Fig. 6: Maximum singular values of \mathbf{M} (top, linear scale on the vertical axis) and of \mathbf{L} (bottom) for the new design (39) for the diagonal and non-diagonal forms of the learning filter transfer-function matrix.

in this paper together with amplitude spectrums of the reference signals (bottom plot). These spectra have many components at low frequencies and therefore the choice of $\omega_{r1} = 10^{-4}$ rad/s and $\omega_{r2} = 0.02$ rad/s were made.

Another advantage of the new design is to complement \mathbf{L} with a limit on its maximum singular value to increase the robustness of the ILC design against measurement noise. The choice of this parameter is application dependent and for this application it is taken as approximately $2.5(\bar{\sigma}(\mathbf{P}))^{-1}$ at the cut-off frequency of the Q -filter and results in $L_{\max} = 50$. Completing the design gives the entries in \mathbf{L} of (42) as

$$\begin{aligned} L_1(q) &= 1.4050q^1 - 1.4796q^2 - 2.6064q^3 - 3.4666q^4 \\ &\quad - 4.3478q^5 - 5.4692q^6 - 6.6882q^7 - 8.2280q^8 \\ &\quad - 10.4490q^9 + 42.3133q^{10}, \\ L_2(q) &= 3.8432q^1 - 1.7307q^2 - 2.7839q^3 - 3.4920q^4 \\ &\quad - 4.3099q^5 - 5.4891q^6 - 6.6589q^7 - 8.0460q^8 \\ &\quad - 10.2179q^9 + 39.8697q^{10}. \end{aligned}$$

Fig. 6 (black solid lines) shows the maximum singular values of \mathbf{M} (top plot) given by (40) and \mathbf{L} (bottom) for this design. The maximum singular values of \mathbf{M} in the range $\omega \in [10^{-4}, 10^{-2}]$ rad are small, which should result in a fast convergence speed of the tracking error. The convergence rate $\gamma = \max(\bar{\sigma}(\mathbf{M}))$ is 0.9, i.e., equal to M_{\max} , due to the first constraint in (39). The maximum gain of the learning filter i.e., $\max(\bar{\sigma}(\mathbf{L}))$ is equal to L_{\max} , due to the second constraint in (39).

All designs in this section has been validated over 10 trials with the zero boundary conditions i.e. $\mathbf{v}_0(p) = \mathbf{0}$ and $\mathbf{e}_0(p) = \mathbf{0}$. The reference trajectories and the disturbance signals are shown in Fig. 7. Also the disturbance signals (given by black and gray dashed line in Fig. 7) are the heat flows generated by the actuators connected to the second and fourth sections of the rod, where these section also contain the measurements of the outputs. The ambient temperature, i.e., the entry in the disturbance vector \mathbf{d}_{k+1}

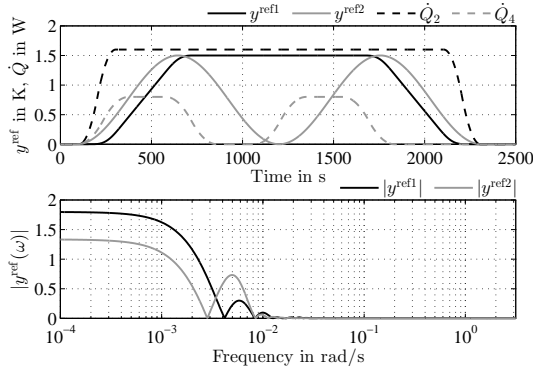


Fig. 7: The reference and disturbance signals (top). Frequency spectrum of the reference signals (bottom).

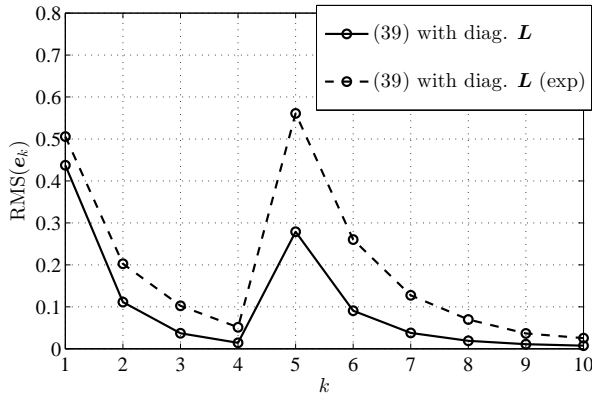


Fig. 8: RMS(e_k) values of the tracking error vector for the new design, where $L(exp)$ denotes the experimentally measured results.

in (12), was set to zero for the simulations. To highlight the compensation properties of the design the disturbance signals were applied starting from the fifth trial, i.e. on trial $k = 5, \dots, 10$.

The root-mean-square, denoted RMS(e_k) of the tracking vector, given by

$$\text{RMS}(e_k) = \sqrt{\frac{1}{\alpha} \sum_{p=1}^{\alpha} e_k^T(p) e_k(p)}$$

is used to compare the trial-to-trial convergence of all the designs in this section, where $\alpha = 2500$ is the trial length.

The black solid line in Fig. 8 shows the RMS(e_k) resulting from the simulation of the controlled system, demonstrating the fast convergence of the tracking error. Also the increase in the error due to the introduction of the disturbance from the 5th trial and for succeeding trials is also quickly and monotonically reduced.

To validate these simulation predictions, an experimental program was also completed. The ILC signals, input signals, output signals and the tracking errors progressions recorded during these experiments are shown in Fig. 9. These show strong agreement with the simulation results as does the experimental RMS(e_k) of the error also shown

in Fig. 8 (black dashed line), where the differences between the simulated and experimental results are due to measurement noise and modelling errors. Moreover, the temperature in the laboratory increased as the experiments progressed, i.e., the ambient temperature changed during the experiments but the simulations assumed a constant ambient temperature.

These results confirm that this ILC design does not require knowledge of the exact plant model and repetitive disturbance signals to achieve precision tracking. Moreover, the effects of non-repetitive, slow-varying disturbances in form of changes of the ambient temperature are compensated by the disturbance observer.

In Fig. 7 $y^{\text{ref1}}(0) = y^{\text{ref2}}(0) = 0$, i.e., equal to the initial ambient temperature at the beginning of the first trial. During the experiment, the ambient temperature increased and at the beginning of subsequent trials $y^{\text{ref1}}(0)$ and $y^{\text{ref2}}(0)$ were lower than the ambient temperature. This means that without the current trial feedback loop, between the end one trial and the start of the next, the rod temperature would change due to changes in the ambient temperature and an initial tracking error would occur starting on the second trial. However, the current feedback control loop, including the disturbance observer, was operating between trials and compensated this unwanted effect, resulting in zero initial error on each trial, see Fig. 9.

It is necessary to compare the new design with alternatives. The first of these designs the ILC law in the absence of a limit on L , i.e. \mathcal{L}_∞ -based optimal synthesis

minimize M

subject to:

$$\begin{aligned} \bar{\sigma}(\mathbf{M}(e^{j\omega_i T_s})) &\leq M, \quad \forall \omega_i \in [\omega_1 < \omega_2 < \dots < \omega_N] \\ M &\leq M_{\max}, \end{aligned} \quad (45)$$

where $\mathbf{M}(e^{j\omega_i T_s})$ is given by (40) and $0 < M_{\max} < 1$ is an appropriately chosen value as in (39). An alternative design is to use (45) with the additional conditions

$$\bar{\sigma}(\mathbf{L}(e^{j\omega_i T_s})) \leq L_{\max}, \quad \forall \omega_i \in [\omega_1 < \omega_2 < \dots < \omega_N] \quad (46)$$

Fig. 10 shows plots of the maximum singular values of the \mathbf{M} and the learning filter for these last two designs.

Another design was completed with the Q -filter as before but a non-diagonal L of the form

$$\mathbf{L}(q) = \begin{bmatrix} L_{11}(q) & L_{12}(q) \\ L_{21}(q) & L_{22}(q) \end{bmatrix}$$

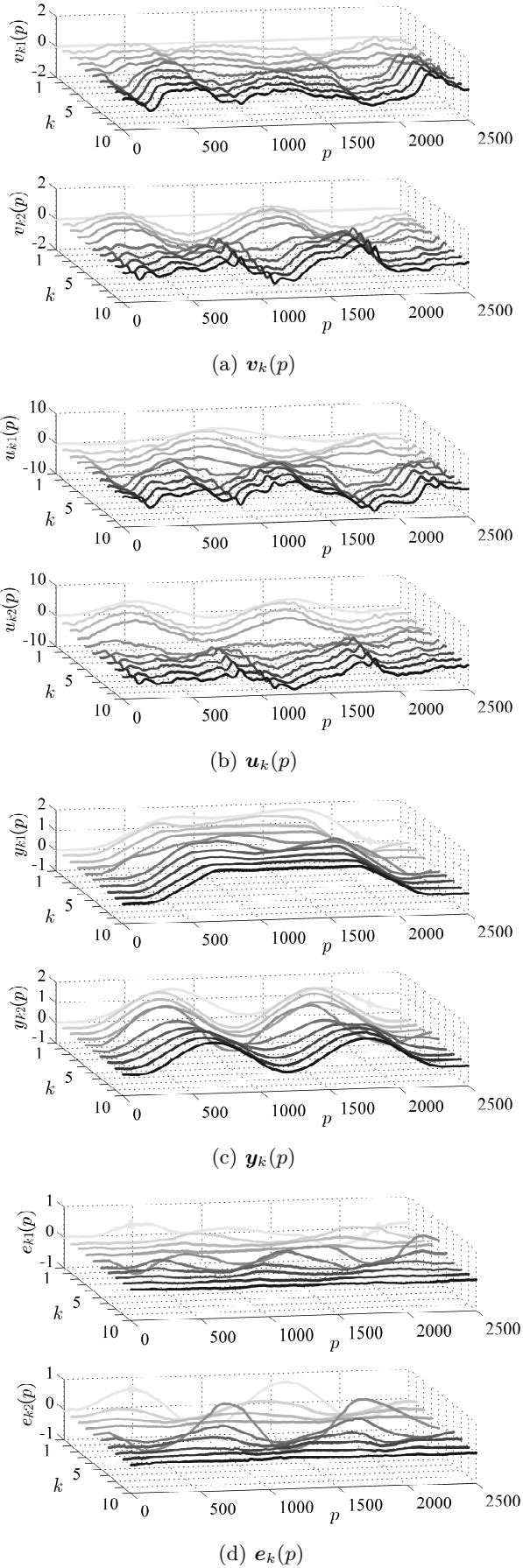


Fig. 9: Experimentally measured signals for the new design.

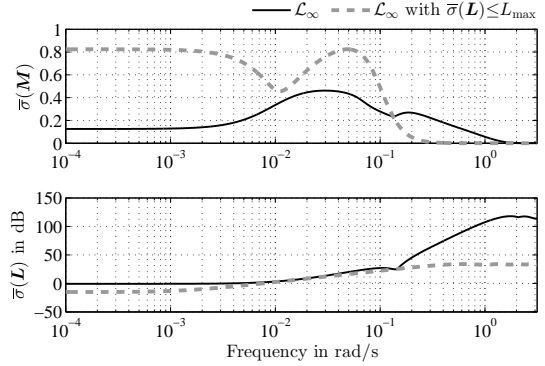


Fig. 10: Maximum singular values of \mathbf{M} (top, linear scale on the vertical axis) and of \mathbf{L} (bottom) for the design based on (45) and for the design based on (45) and (46).

resulting in

$$\begin{aligned}
 L_{11}(q) &= 1.9762q - 2.3071q^2 - 3.0377q^3 - 3.5838q^4 \\
 &\quad - 4.2453q^5 - 5.2667q^6 - 6.2530q^7 - 7.4311q^8 \\
 &\quad - 9.2380q^9 + 40.3817q^{10}, \\
 L_{12}(q) &= 2.7801q + 0.6410q^2 + 0.4889q^3 + 0.4967q^4 \\
 &\quad + 0.4305q^5 + 0.1898q^6 - 0.0117q^7 - 0.3192q^8 \\
 &\quad - 1.1067q^9 - 3.5864q^{10}, \\
 L_{21}(q) &= 4.5104q - 0.1022q^2 - 0.3272q^3 - 0.3833q^4 \\
 &\quad - 0.4523q^5 - 0.6748q^6 - 0.7047q^7 - 0.6607q^8 \\
 &\quad - 0.6644q^9 - 0.5390q^{10}, \\
 L_{22}(q) &= -0.7430q - 2.5071q^2 - 3.0921q^3 - 3.6281q^4 \\
 &\quad - 4.2474q^5 - 5.0970q^6 - 6.0247q^7 - 7.1572q^8 \\
 &\quad - 8.7486q^9 + 42.2384q^{10}.
 \end{aligned}$$

The gray dashed plots in Fig. 6 show the maximum singular values of \mathbf{M} and the learning filter for this design.

For comparison purposes, the simulation results for the alternative ILC designs and also for the case when the ILC loop is disabled, i.e., $\mathbf{v}_{k+1}(p) = \mathbf{0}$. The $\text{RMS}(e_k)$ values for these designs against trial number shown in Fig. 11, where in the case when the ILC loop is disabled the constant values of $\text{RMS}(e_k)$ before and after the start of disturbance generation on the fifth trial are typical for control systems without learning algorithms.

The \mathcal{L}_∞ -based design, i.e. (45), results in a very fast trial-to-trial error convergence speed, however, the maximum singular values of the learning filter for high frequencies are large. Implementing this design on a physical system can make it sensitive to measurement noise and initial conditions. For the design based on using (45) and (46), the maximum singular values of \mathbf{L} stays below the limit $L_{\max} = 50$ but the maximum singular values of \mathbf{M} for low frequencies are large. This, in turn, results in a (relatively) slow trial-to-trial error convergence speed and the disadvantages of the both \mathcal{L}_∞ -based designs have been overcome in the new design (39).

The gray dashed line in Fig. 11 shows $\text{RMS}(e_k)$ values for the new design (39) with the non-diagonal form of \mathbf{L} .

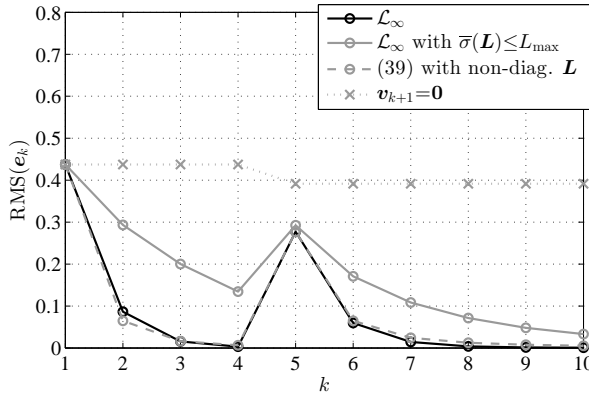


Fig. 11: RMS(e_k) values of the three ILC designs plus the case when the ILC loop is disabled.

The convergence speed of this design is slightly higher than that for the diagonal form of \mathbf{L} (see the black solid plot in Fig. 8) and is comparable to the \mathcal{L}_∞ -based design despite $\max(\bar{\sigma}(\mathbf{L}(e^{j\omega_i T_s}))) = 50$ (see Fig. 6, bottom plot, gray dashed line).

V. CONCLUSIONS

An ILC design method for a multivariable distributed parameter systems based on first constructing a finite-dimensional model described by linear ordinary differential equations has been developed and experimentally validated. This design uses a current trial feedback control loop to achieve good tracking performance starting from the first trial and compensation of non-repetitive disturbances by inclusion of a disturbance observer. The current trial feedback control loop is also designed to reduce the coupling in the system, which allows for the use a simplified, i.e., diagonal form of the Q -filter and the learning filter, as a comparison a non-diagonal learning filter was also designed but gave relatively little relative improvement in performance.

In this new design, the ILC filters are designed in the frequency domain and based on convex optimization. The ILC filters can be either non-causal or causal and the choice of the orders of these filters is based on knowledge of the particular example under consideration. To provide fast trial-to-trial error convergence rate of over a specified frequency range or to limit the maximum gain (i.e., the maximum singular value) of the learning filter the use of weighting functions is not needed. Overall, the frequency domain design requires the designer to specify several scalar parameters. The performance of this design has been confirmed by experimental application to the heating process, where changes in the ambient temperature of the laboratory during the experiments allows validation of the attenuation of non-repetitive disturbances.

The new design is based on first constructing a finite-dimensional approximation to the distributed parameter dynamics and the approximation has been constructed using one of a number of alternatives. Investigation of

the potential, together with examining the relative performance, of others is one area for possible future research as is application of the design to other distributed parameter systems. Moreover, by the disturbance observer, this new design has the capability to reject non-repetitive disturbances and further work is required to extend to stochastic disturbances.

REFERENCES

- [1] D. A. Bristow, M. Tharayil, and A. G. Alleyne. A survey of iterative learning control. *IEEE Control Systems Magazine*, 26(3):96–114, 2006.
- [2] H.-S. Ahn, Y.-Q. Chen, and K. L. Moore. Iterative learning control: Brief survey and categorization. *IEEE Transactions on Systems, Man and Cybernetics, Part C*, 37(6):1099–1121, 2007.
- [3] O. Sörnmo, B. Bernhardsson, O. Kröling, P. Gunnarsson, and R. Tenghamn. Frequency-domain iterative learning control of a marine vibrator. *Control Engineering Practice*, 47:70–80, 2016.
- [4] T. Oomen and C. R. Rojas. Sparse iterative learning control with application to a wafer stage: Achieving performance, resource efficiency, and task flexibility. *Mechatronics*, 47:134–147, 2017.
- [5] S. Mandra, K. Galkowski, E. Rogers, A. Rauh, and H. Aschemann. Performance-enhanced robust iterative learning control with experimental application to PMSM position tracking. *IEEE Transactions on Control Systems Technology*, 27(4):1813–1819, 2019.
- [6] D. Huang, X. Li, J.-X. Xu, C. Xu, and W. He. Iterative learning control of inhomogeneous distributed parameter systems—frequency domain design and analysis. *Systems & Control Letters*, 72:22–29, 2014.
- [7] R. W. Lewis, P. Nithiarsu, and K. N. Seetharamu. *Fundamentals of the Finite Element Method for Heat and Fluid Flow*. Wiley, 2004.
- [8] A. Rauh, L. Senkel, H. Aschemann, V. V. Saurin, and G. V. Kostin. An integrodifferential approach to modeling, control, state estimation and optimization for heat transfer systems. *International Journal of Applied Mathematics and Computer Science*, 26:15–30, 2016.
- [9] L. Blanken, J. Willems, S. Koekebakker, and T. Oomen. Design techniques for multivariable ILC: Application to an industrial flatbed printer. In *7th IFAC Symposium on Mechatronic Systems*, pages 213–221, 2016.
- [10] M. Tomizuka. Zero phase error tracking algorithm for digital control. *Journal of Dynamic Systems, Measurement, and Control*, 109(1):65–68, 1987.
- [11] D. De Roover and O. H. Bosgra. Synthesis of robust multivariable iterative learning controllers with application to a wafer stage motion system. *International Journal of Control*, 73(10):968–979, 2000.
- [12] K. Inaba, C.-C. Wang, M. Tomizuka, and A. Packard. Design of iterative learning controller based on frequency domain linear matrix inequality. In *2009 American Control Conference*, pages 246–251, June 2009.
- [13] T. D. Son, G. Pipeleers, and J. Swevers. Multi-objective iterative learning control using convex optimization. *European Journal of Control*, 33:35–42, 2017.
- [14] S. Mandra, K. Galkowski, E. Rogers, H. Aschemann, and A. Rauh. Iterative learning control of a distributed heating system described by a non-minimum phase model. In *2018 American Control Conference (ACC)*, pages 5606–5611, 2018.
- [15] H. Aschemann and A. Rauh. An integro-differential approach to control-oriented modelling and multivariable norm-optimal iterative learning control for a heated rod. In *2015 20th International Conference on Methods and Models in Automation and Robotics (MMAR)*, pages 447–452, 2015.
- [16] F. Incropera, D. P. DeWitt, T. L. Bergman, and A. S. Lavine. *Fundamentals of Heat and Mass Transfer*. Wiley, 2007.
- [17] H. Aschemann, A. Rauh, G. Kostin, and V. Saurin. Multivariable temperature control of a heated rod by using a reduced-order internal MIDR-model. In *American Control Conference*, pages 1772–1777, 2018.

- [18] J.-H. She, H. Kobayashi, Y. Ohyama, and X. Xin. Disturbance estimation and rejection — an equivalent input disturbance estimator approach. In *43rd IEEE Conference on Decision and Control*, volume 2, pages 1736–1741, 2004.
- [19] M. Norrlöf and S. Gunnarsson. Time and frequency domain convergence properties in iterative learning control. *International Journal of Control*, 75(14):1114–1126, 2002.
- [20] D. H. Owens, B. Chu, E. Rogers, C. T. Freeman, and P. L. Lewin. Influence of nonminimum phase zeros on the performance of optimal continuous-time iterative learning control. *IEEE Transactions on Control Systems Technology*, 22(3):1151–1158, 2014.